1957

A study of divergence at 300 mbs.

Bechelmayr, Leroy R.

Monterey, California: Naval Postgraduate School, 1957.

A STUDY OF DIVERGENCE AT 300 mbs

Leroy R. Bechelmayr

7

A STUDY OF DIVERGENCE AT 300 MBS

****

Leroy R. Bechelmayr

A STUDY OF DIVERGENCE AT 300 MBS

by

Leroy R. Bechelmayr

Lieutenant Junior Grade, United States Navy

Submitted in partial fulfillment of
the requirements for the degree of

MASTER OF SCIENCE
IN

AEROLOGY

United States Naval Postgraduate School
Monterey, California

1 9 5 7

A STUDY OF DIVERGENCE AT 300 MBS

by

Leroy R. Bechelmayr

This work is accepted as fulfilling
the thesis requirements for the degree of
MASTER OF SCIENCE
IN
AEROLOGY

from the
United States Naval Postgraduate School

ABSTRACT

Computation of the terms of the vorticity equation is made at 300 mbs using the assumption that vertical motions are negligible and approximating relative vorticity by geostrophic vorticity computed from finite differences. The validity of the computations is then tested, giving good qualitative agreement but poor statistical agreement. The isobaric divergence at 300 mbs as computed using $\frac{\partial u}{\partial x}+\frac{\partial v}{\partial y} = \nabla_p \cdot \underline{V}$ is compared with the value of divergence as obtained from the vorticity equation. Again there was only qualitative agreement. The magnitude of the lateral and longitudinal components of isobaric divergence were studied and it was found that the lateral component was dominant in 75 per cent of the cases studied. No relationship was found between the longitudinal component and the total divergence. The synoptic aspects of the divergence fields at 300 mbs are discussed with respect to the 500-mb surface.

The writer wishes to express his appreciation for the guidance and encouragement given him by Professor F. L. Martin of the U.S. Naval Postgraduate School in this investigation.

LIST OF ILLUSTRATIONS

LIST OF SYMBOLS USED

x, y, z, - Rectangular (Cartesian) coordinates; standard coordinates with x axis toward the east, y axis toward the north, z axis toward the zenith.

$\underline{i}, \underline{j}, \underline{k}$ - Rectangular (Cartesian) system of unit vectors along x, y and z axes.

ζ_a = Vertical component of absolute vorticity.

$\frac{d}{dt}$ = A three dimensional time rate of change operator.

$\underline{\nabla}_p$ = Gradient operator on an isobaric surface.

$\underline{V}$ = Wind velocity vector.

$\underline{\nabla}_p \cdot \underline{V}$ = Isobaric divergence

ω = $\frac{dp}{dt}$ - Rate of change of pressure of an air particle with time.

$\frac{\partial}{\partial p}$ = Local rate of change operator with respect to pressure.

$\underline{V}_H$ = Horizontal component of wind vector.

$\frac{D}{Dt}$ = Time rate of change operator along an isobaric surface.

g = Acceleration due to gravity (32.17 feet per second per second).

f = Coriolis parameter ($2 \Omega \sin \varphi$).

Ω = Angular speed of the earth (7.292×10^{-5} radians per second).

φ = Latitude

z = Height of an isobaric surface.

$\nabla^2 z$ = Laplacian of height.

u, v, w = Components of wind velocity along the x, y and z axes respectively.

$\bar{z}$ = Space-averaged height of an isobaric surface.

d = Grid distance (2.5° of latitude $= 9.12 \times 10^5$ feet)

β = $\frac{df}{dy}$ = Rate of change of coriolis parameter along the y axis.

ψ = Angle between wind velocity and the gradient of $(\bar{z}-z)$.

ρ = Density of the air.

$\underline{s},\underline{n},\underline{k}$ - Natural system of unit vectors.

α = Wind direction.

r = Correlation coefficient.

cov(xy) = Covariance of stochastic variables x and y.

S = Standard deviation of a stochastic variable.

S^2 = Variance of a stochastic variable.

n = Size of a statistical sample.

TABLE OF CONTENTS

1. Introduction.

Several studies of divergence in the atmosphere have been carried out by different methods and by different investigators. Some of the most notable of these are Fleagle [2], Arnason [1], and Landers [5]. Their investigations have involved a three dimensional study of the distribution of divergence in the atmosphere. Landers [5] computed horizontal divergence using constant level charts and a "del computer" which consists of computing divergence from the wind vectors at the vertices of an equilateral triangle with an altitude of $2\frac{1}{2}^{\circ}$ of latitude. Arnason [1] computed the integrated divergence over a 12 hour period in isobaric layers with the use of vertical velocities, the local rate of change of thickness and the temperature advection. Fleagle computed horizontal velocity divergence and mass divergence up to about 150 mbs and found a level of non-divergence at about 600 mbs.

This study is carried out at 300 mbs only and no attempt is made to extend it to three dimensions. The main objective of this study was to gain some practical knowledge of the behavior of divergence patterns and to apply the results to the prognoses of the 500-mb chart. Computations of the divergence and the individual rate of change of the absolute vorticity with time are made, and their relationship tested. Also a study of the relationship between the longitudinal component of the divergence and the isobaric divergence is made.

2. Source of Data.

A series of 300-mb maps, carefully analyzed by the staff of the U.S. Naval Postgraduate School, was used in making the computations. The analyses employed were those of 1500Z, 15 November, 0300Z and 1500Z, 16 November 1955. On the first chart there is a trough and a closed low at about 112° W and a ridge at about 84° W with considerable meridional flow. At 0300Z on the 16th the trough and ridge have moved about 5° eastward, retaining about the same intensity. By 1500Z on the 16th the amplitude of the trough-ridge system has decreased considerably and moved to 98° W and 72° W longitude so that in between the trough and ridge the flow is becoming zonal. Computations, which will be described in the following sections, were carried out between this trough and ridge. In addition some computations were made behind the trough on the 0300Z, 16 November chart. A total of 138 computations of all five terms of Equation (7) below were made.

3. Mathematical Analysis.

The vorticity equation in isobaric coordinates is:

$$(1) \qquad \frac{d f_a}{dt} = -f_a(\nabla_p \cdot \underline{V}) - \underline{k} \cdot \nabla_p \omega \times \frac{\partial \underline{V}}{\partial p}$$

This is not in the form in which computations from a synoptic chart can be readily made. Since vertical velocities are normally small, the second term on the right side

of the equation may be ignored. Equation (1) then becomes the approximation to the vorticity equation as it is commonly made in meteorology.

$$(2) \qquad \frac{D\zeta_a}{Dt} = -\zeta_a (\nabla_p \cdot \underline{V})$$

Making the geostrophic approximation, $\zeta = \frac{g}{f} \nabla^2 z$, and noting that the coriolis parameter does not change with time, Equation (2) becomes:

$$(3) \qquad \frac{D}{Dt}\left(\frac{g}{f}\nabla^2 z + f\right) = -\left(\frac{g}{f}\nabla^2 z + f\right)(\nabla_p \cdot \underline{V})$$

In order to compute the individual rate of change of vorticity it would be necessary to construct isobaric trojectories of the air parcels. However, such computations may be avoided by making use of the fact that:

$$(4) \qquad \frac{D\zeta_a}{Dt} = \frac{\partial \zeta_a}{\partial t} + \underline{V}_H \cdot \nabla_p \zeta_a$$

Equation (3) then becomes:

$$(5) \qquad \frac{\partial}{\partial t}\left(\frac{g}{f}\nabla^2 z\right) + \underline{V}_H \cdot \nabla_p \left(\frac{g}{f}\nabla^2 z\right) + v\frac{df}{dy} = -\left(\frac{g}{f}\nabla^2 z + f\right)\left(\nabla_p \cdot \underline{V}_H\right)$$

Since $\frac{g}{f}$ is quasi-constant compared to the horizontal variation of $\nabla^2 z$, it may be brought outside of the differential operator in the second term of the left side of Equation (5). In order to get $\nabla^2 z$ in a form in which computations can be made, finite differences may be used to give:

$$(6) \qquad \nabla^2 z = \frac{\bar{z} - z}{d^2}$$

Combining Equations (5) and (6) and multiplying by $\frac{fd^2}{g}$ gives:

$$(7)\quad \underbrace{\frac{\partial}{\partial t}(\bar{z}-z)}_{a} + \underbrace{\underline{V}_H \cdot \underline{\nabla}_p(\bar{z}-z)}_{b} + \underbrace{\frac{fd^2}{g}\beta v}_{c} = \underbrace{-\left[(\bar{z}-z) + \frac{f^2d^2}{g}\right]}_{d}\underbrace{(\underline{\nabla}_p \cdot \underline{V})}_{e}$$

The equation is now in a form in which computations were made. The left hand side of this equation now represents $\frac{fd^2}{g}\frac{D\zeta_a}{Dt}$ and the right hand side represents $-\frac{fd^2}{g}\zeta_a(\underline{\nabla}_p \cdot \underline{V})$. By measuring wind velocities in feet per second and grid distances in feet, the units of this equation can be shown to be feet per second.

4. Computational Procedure.

The quantity $\bar{z}$ may be readily computed using a grid as shown in Figure 1.

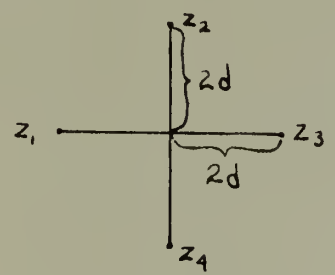

Figure 1

Grid for computing space mean.

The value of 2d was chosen to be 5° of latitude. This value is about half of the length of the short-wave trough so that in constructing a z-chart, the short-wave troughs tend to be removed, but the long-wave troughs are unaffected.

The construction of the $\bar{z}$-chart where $\bar{z}$ is $\frac{z_1+ z_2+ z_3+ z_4}{4}$ (Figure 1), was accomplished by displacing two z-charts 10 degrees of latitude laterally and adding graphically giving $z_1+ z_3$. The two maps were then displaced 10 degrees of latitude northward and added giving z_2+z_4. The z_1+z_3 contours are then added to the z_2+z_4 contours giving $4\bar{z}$. By dividing by 4 we then have a space mean map from which the actual map may be graphically subtracted giving isolines of $(\bar{z}-z)$. The local rate of change of $(\bar{z}-z)$ was approximated by the average rate of change in the quantity over a 12-hour interval, as measured at any given station.

The advection term [term (b)] was computed by measuring (1) the gradient of $(\bar{z}-z)$ across selected stations over a distance of 5° of latitude, (2) the wind velocity in feet per second, and (3) the angle ψ between the wind vector and the gradient vector. The magnitude of term (b) is then $|V|\,|\nabla_p(\bar{z}-z)|\,|\cos\psi|$. A diagram of the vectors involved is shown in Figure 2.

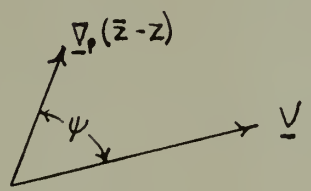

Figure 2

Diagram of Angle ψ

All factors of term (c) with the exception of v are constant for a given latitude and can be computed for each

latitude circle. Taking the appropriate value of $\frac{fd^2}{g}\beta$ and multiplying by the northward component of the wind velocity gives the final term in the vorticity computation. Now by equation (7) the sum of terms (a), (b) and (c) represent the quantity $\frac{fd^2}{g}\frac{D\mathcal{J}_a}{Dt}$ subject to the accuracy of the approximations made in neglecting vertical motions and in computing $\frac{\partial}{\partial t}(\bar{z}-z)$.

Several methods have been devised for computing isobaric divergence [3, 6]. It was decided to use the following equation in the computation.

$$(8)\quad \nabla_p \cdot \underline{V} = \frac{\partial u}{\partial x} + \frac{\partial v}{\partial y}$$

A square grid $2\frac{1}{2}$ degrees of latitude on a side was used. An average u was computed on each side of the square and an average v at the top and bottom. As shown in Figure 3, the isobaric divergence is then $\frac{u_2-u_1}{d}+\frac{v_2-v_1}{d}$.

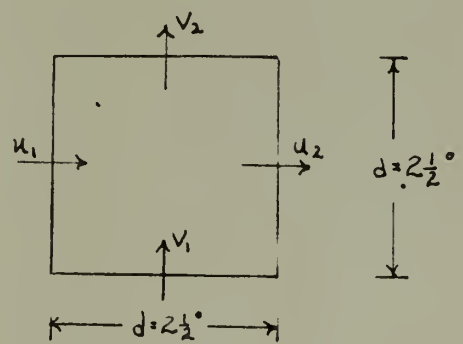

Figure 3

Grid for computing divergence.

Since the grid is square no spherical correction is necessary, and grids can be oriented along the major flow. If the values of isobaric divergence are then multiplied

by term (d) of Equation (7) the value should be the same as the sum of terms (a), (b) and (c). The divergence was also computed by dividing the sum of terms (a), (b) and (c) by term (d) of Equation (7). For the discussion in this paper this value of isobaric divergence will be referred to as <u>effective divergence</u>.

Isolines of the computed values of $\frac{fd^2}{g}\frac{D\rho_a}{Dt}$ are plotted in Figures 4, 8 and 12. The isolines of $-\frac{fd^2}{g}\rho_a(\nabla_p \cdot \underline{V})$ are drawn in Figures 5, 9 and 13. The field of effective divergence is plotted in Figures 6, 10 and 14, and isobaric divergence is plotted in Figures 7, 11 and 15. The labeled values of isolines of $\frac{fd^2}{g}\frac{D\rho_a}{Dt}$ and $-\frac{fd^2}{g}\rho_a(\nabla_p \cdot \underline{V})$ are times 10^{-3} and the labeled values of the fields of divergence are times 10^{-5}. In plotting the values of isobaric divergence in Figure 7 the values in four adjacent squares were averaged and then plotted in the common point of the four squares. This was done in an effort to smooth the divergence field but was not done in Figures 11 and 15 because the averaging could mask the effects of short waves.

5. The Results of the Computations.

The individual terms on the right hand side of Equation 7 have order of magnitude $= 10^{-3}$ feet per second. A typical value of the change of $(\bar{z}-z)$ over a twelve hour period is ± 100 feet. When divided by 12 hours or 4.32×10^4 seconds,

$\frac{\partial}{\partial t}(\bar{z}-z)$ has a value of about $\pm$ 2.3 x 10^{-3} feet per second. The extreme computed value of $\frac{\partial}{\partial t}(\bar{z}-z)$ was 11.6 x 10^{-3} feet per second. Measuring $|\nabla_p(\bar{z}-z)|$ over a distance of 5° of latitude (2½° each side of the station) gives values of the order of 5.0 x 10^{-5}. With a wind of 120 feet per second and an angle ψ whose cosine is 0.3, a typical value of term (b) is 1.8 x 10^{-3} feet per second. The maximum magnitude of this term was 20.5 x 10^{-3} feet per second. The quantity $\frac{fd^2\beta}{g}$ ranges from 11.4 x 10^{-6} at 30° and 60° N to 13.18 x 10^{-6} at 45° N where it is maximum. When multiplied by a typical value of 100 feet per second for v, one obtains a value for term (c) of 1.1 x 10^{-3} to 1.3 x 10^{-3} feet per second. The maximum value of term (c) was 1.87 x 10^{-3} feet per second. Although term (c) is of the same order of magnitude as terms (a) and (b), it is somewhat smaller in general and terms (a) and (b) give the largest contribution to the sum of the three terms of the left side of Equation (7).

The value of $\frac{f^2d^2}{g}$ is constant for a given latitude circle and ranges from 1.37 x 10^2 feet at 30° N to 3.66 x 10^2 feet at 55° N, while $(\bar{z}-z)$ ranges from -300 feet to 300 feet. Term (d) was positive in all the computations except one, in which it was a small negative value. Of course all computations were carried out in the broad scale flow between trough and ridge. Term (d) could very well be a negative value in a closed high pressure system where values of $(\bar{z}-z)$ might be as great as -400 feet.

Values of isobaric divergence were in general smaller

than those of effective divergence. However they agree fairly well qualitatively. The magnitude of the effective divergence agrees very well with that computed by Landers [5]. The average absolute value of the effective divergence on the three charts was 3.34, 3.70 and 1.22 all times 10^{-5} per second. A plot of divergence values versus height was made by Landers [5] and shows an increase of 0.6×10^{-5} per second in the mean absolute value of horizontal divergence from 20,000 to 25,000 feet. Extrapolation of his curve to 30,000 feet would give a value of 2.7×10^{-5} per second, and the mean absolute value of effective divergence of all the computation made in this study is 2.78×10^{-5} per second. The values of isobaric divergence have a maximum magnitude of about 3.5×10^{-5} per second while the mean absolute value is about 1.0×10^{-5} per second which agrees better with the values of divergence as computed by Arnason [1]. In the following section a statistical approach is made in comparing the two fields of divergence and the fields of $\frac{fd^2}{g} \frac{D\rho_a}{Dt}$ and $-\frac{fd^2}{g} \rho_a (\nabla_p \cdot \underline{V})$.

6. Statistical Studies.

Of the patterns of $\frac{fd^2}{g} \frac{D\rho_a}{Dt}$ and $-\frac{fd^2}{g} \rho_a (\nabla_p \cdot \underline{V})$ Figures 12 and 13 seem to give the best agreement. To test this agreement a correlation coefficient of the two quantities was found using values at 35 points in each figure. This correlation coefficient r is given by the following equation

from Hoel [4].

(9) $$r = \frac{\text{cov}\,(xy)}{S_x S_y}$$

Cov(xy) is the covariance of x and y, the stochastic variables, and S_x and S_y are the respective standard deviations. Cov(xy) and the standard deviations were computed from the following equations given in [4].

(10) $$\text{cov}(xy) = \frac{1}{n}\left[\Sigma xy - n\bar{x}\bar{y}\right]$$

(11) $$S_x^2 = \frac{1}{n}\left[\Sigma x^2 - \frac{1}{n}(\Sigma x)^2\right]$$

(12) $$S_y^2 = \frac{1}{n}\left[\Sigma y^2 - \frac{1}{n}(\Sigma y)^2\right]$$

The mean value of $\frac{fd^2}{g}\frac{D\varphi_a}{Dt}$ was -2.06×10^3 feet per second and the mean value of $-\frac{fd^2}{g}\varphi_a(\nabla_p \cdot \underline{V})$ was 0.1×10^{-3} feet per second. The standard deviations were 6.38×10^{-3} feet per second and the 3.52×10^{-3} feet per second respectively. The correlation coefficient was found to be 0.31. With 90 per cent confidence limits the critical value of r is 0.29 so the correlation coefficient of 0.31 is significant at this level of confidence. However, the value of r is not large enough to deduce more than that the two quantities are related. Some of the reasons for this lack of agreement will be discussed later.

The same procedure as described in the previous paragraphs was used to compute a correlation coefficient between Figures 10 and 11 which are patterns of effective divergence

and isobaric divergence. It was believed that perhaps better agreement could be achieved between these two patterns since in the process of dividing $\frac{D f_a}{Dt}$ by $-f_a$ some of the errors in using the geostrophic approximation might be minimized. However, the correlation coefficient between Figures 10 and 11 was only 0.144 which is significant at 68 per cent confidence limits with a sample size of 52.

The approximation of $\frac{\partial}{\partial t}(\bar{z}-z)$ by a 12-hour average would tend to cause a computed effective divergence center to be east of its instantaneous position if the future 12-hour $(\bar{z}-z)$ map is used and west of its instantaneous position if the previous 12-hour $(\bar{z}-z)$ map is used. The plotted values of effective divergence and isobaric divergence were examined in an attempt to find some consistent displacement which would give a higher correlation coefficient. It was believed that the correlation coefficient could be improved by shifting the divergence center over Indiana in Figure 10 into coincidence with the divergence center over Michigan in Figure 11 while the convergence centers over Iowa remained in coincidence. Actually, however, there was no improvement in the correlation coefficient. A value of 0.07 was computed for r with a sample size of 31 which is not significant at any reasonable level of confidence.

Sutcliffe [7] has stated that the vortex-tube term in the vorticity equation tends to be offset by $-f(\underline{\nabla}_p \cdot \underline{V})$ so that a better approximation to the vorticity equation would be:

(13) $$\frac{D\zeta_a}{Dt} = -f(\nabla_p \cdot \underline{V})$$

A correlation coefficient was computed using this approximation and the computations from the 1500Z, 16 November chart. Using Equations (9), (10), (11) and (12) the correlation coefficient was computed to be -0.204 which is significant at 75 per cent confidence limits. The fact that the correlation coefficient is negative seems to indicate that ignoring $f(\nabla_p \cdot \underline{V})$ must overcompensate for the vortex-tube term.

Using the equation for isobaric divergence in natural coordinates:

(14) $$\nabla_p \cdot \underline{V} = V\frac{\partial \alpha}{\partial n} + \frac{\partial V}{\partial s}$$

it is seen that there are two components of the total divergence, a longitudinal component along a streamline and a lateral component normal to the streamline. It was also of interest to determine which of these components gives the greatest contribution to the total isobaric divergence. The rate of change of wind velocity along a streamline is most easily measured and was found at all the stations at which vorticity computations were made. This was done by measuring the change in wind speed along a streamline for a distance 5° of latitude across each station. If these values are compared with the effective divergence, the difference will be the effective lateral component. In most cases the lateral and longitudinal

terms are of opposite sign. In 103 out of 138 computations (approximately 75%) the lateral term was the dominant term. Therefore, most of the time the sign of the effective divergence is determined by the effective lateral component.

It would be helpful if some relationship could be derived between effective divergence and the longitudinal component since the longitudinal component can be easily measured. The total divergence could then be determined simply by measuring $\frac{\partial V}{\partial s}$. Using Equations (9), (10), (11) and (12) to determine a correlation coefficient between $\frac{\partial V}{\partial s}$ and the effective divergence gave a coefficient of 0.087 which is not significant at any reasonable level of confidence. Therefore, very little about the magnitude of the effective divergence can be deduced from the magnitude of the longitudinal divergence.

7. Sources of Error.

The discrepancy which exists between computed values of $\frac{fd^2}{g}\frac{D\zeta_a}{Dt}$ and $-\frac{fd^2}{g}\zeta_a(\nabla_p \cdot \underline{V})$ and between effective and isobaric divergence is due partially to the fact that the vortex-tube term and the vertical advection of vorticity have been ignored. However, the discrepancy is greater than the values to be expected from the terms that have been ignored. Due to the lack of actual wind reports at 300 mbs, it was necessary to interpolate between the actual wind observations. Error could have been introduced here. Also a 10^{o} error in the

observed wind direction and a 5-knot error in wind speed may cause a maximum error of 3.0×10^{-5} per second in the computed isobaric divergence while the same error in wind direction and speed will cause only an error of 0.34×10^{-5} in the effective divergence. However, there is another approximation in the use of the vorticity equation. This was the determination of $\frac{\partial}{\partial t}(\bar{z}-z)$ as a 12-hour average using two consecutive $(\bar{z}-z)$-charts. The magnitude of the errors due to this approximation is unknown.

8. Synoptic Aspects.

It was difficult to determine the track of the divergence centers as many of them disappeared or were out of the area of computations in the 12-hour intervals. For example, in the 12-hour interval from Figure 6 to Figure 10, three divergence centers have appeared where there was previously only one.

The effective divergence patterns give good qualitative agreement with the synoptic situation. Fleagle [2] has found the 500-mb level to be approximately a level of non-divergence and the 300-mb surface is near the level of maximum divergence. Landers [5] also found the 300-mb level to be a level of maximum divergence and the 500-mb level to be a level of least divergence. Arnason's results [1] did not show such a distribution of divergence, but it is believed that the isobaric divergence as computed at 300 mbs may give a good indication of rises and falls of the 500-mb surface. In Figure 6 the

areas of effective divergence between trough and ridge are relatively large and clear cut. With this divergence pattern aloft we would expect the trough to continue to move eastward, which actually occurs. Figure 7 does not give this same agreement as there is a convergence center centered over station 534 which is behind the ridge. This would indicate retrogression of the ridge which does not occur. It may also be noted in Figure 6 that as the strong winds east of the ridge at 84° W enter the cyclonically curved isohypses of weaker gradient there is a change from convergence to divergence. On the left hand side of Figure 6 there appears to be a perturbation leaving the long-wave trough as indicated by the divergence center over Colorado. As yet there is no actual short-wave trough indicated at 500 mbs. On the next 500-mb chart, 0300Z 16 November, a short-wave trough has appeared east of the long-wave trough. Figures 10 and 11 indicate closed divergence centers ahead of the short-wave trough and closed convergence centers behind it. With the short-wave trough in the broad scale flow, the pattern of divergence is much more complicated and the gradients are much greater. On the West Coast in Figures 10 and 11 there is a center of convergence located ahead of a short-wave trough. Twelve hours later the trough is practically non-existant. The divergence center located over Oregon may be associated with the trough that appears off the West Coast on the 1500Z 16 November chart. In Figures 14 and 15 the short-wave trough of Figures 10 and 11 has

moved into the ridge and weakened. Consequently the divergence and convergence centers that were associated with it are not as clear cut. The patterns have become elongated along the contours with considerable convergence east of the trough. Therefore, the trough may be expected to decrease in amplitude and the flow to become more zonal, which is verified on the 0300Z, 17 November 500-mb chart.

Due to the fact that the surface maps are two and a half hours earlier than the upper-air charts, it is difficult to compare divergence patterns with the surface maps. However, in the few cases studied the low-pressure centers at the surface move toward the centers of divergence at 300 mbs. It is also interesting to note that areas of divergence tend to overlay the fronts at the surface.

9. Summary and Conclusions.

This investigation of the isobaric divergence patterns at 300 mbs has shown that the technique of computing divergence from the rate of change of absolute vorticity gives very good agreement in magnitude with the computations of isobaric divergence made by Landers [5]. The computations made in this investigation indicate that a mean absolute value of divergence at 300 mbs is about 2.8×10^{-5} per second. This value of effective divergence acting over a column of air 12,000 feet thick for a period of 12 hours will cause a fall in the 500-mb surface of about 200 feet. The values of effective divergence plotted in Figures 6, 10 and 14 give good indications of future areas of rise and fall at the

500-mb surface.

The computations of isobaric divergence using Equation (8) gave a smaller mean value, which gives good agreement with the magnitudes computed by Arnason [1]. Except in Figure 7, these values of divergence also give good indications of future developments on the 500-mb surface.

There were rather poor statistical correlation coefficients between computed values of $\frac{fd^2}{g}\frac{D\rho_a}{Dt}$ and $-\frac{fd^2}{g}\rho_a(\nabla_p \cdot \underline{V})$, and also between effective and isobaric divergence. This poor agreement is believed due largely to errors in, and insufficient, wind reports at 300 mbs. Also the 12-hour approximation of $\frac{\partial}{\partial t}(\bar{z}-z)$ introduces error.

The lateral component of the effective divergence was the dominant component in 75% of the computations made. There was found to be no relationship between the effective divergence and either the lateral or longitudinal component of divergence.

BIBLIOGRAPHY

1. Arnason, G., "A Case Study of the Fields of Large Scale Vertical Velocity and Horizontal Divergence", Technical Report No. 16, Office of Naval Research, Massachusetts Institute of Technology, Cambridge, Mass., 38 pp., May 1955.

2. Fleagle, R.G., "Quantitative Analysis of Factors Influencing Pressure Change", Journal of Meteorology, Vol. 5, 281-292, December 1948.

3. Graham, R.D., "A New Method of Computing Vorticity and Divergence", Bulletin of American Meteorological Society, Vol. 34, 68-74, 1953.

4. Hoel, P.G., "Introduction to Mathematical Statistics", John Wiley and Sons, Inc., New York, 1947.

5. Landers, H., "A Three Dimensional Study of the Horizontal Velocity Divergence", Journal of Meteorology, 415-427, October 1955.

6. Panofsky, H.A., "Large Scale Vertical Velocity and Divergence", Compendium of Meteorology, American Meteorological Society, 639-646, Boston 1951.

7 Sutcliffe, R.C., "A Contribution to the Problem of Development", Quarterly Journal of the Royal Meteorological Society, Vol. 73, 370-383, 1947.

FIGURE 4

1500Z 15 NOVEMBER 1955

$\frac{fd^2}{g}\frac{D\delta_a}{Dt} \times 10^3$ $\frac{ft}{sec}$

FIGURE 5

1500 Z 15 NOVEMBER 1955

$-\frac{fd^2}{g}\rho_a(\nabla_p \cdot \underline{V}) \times 10^3 \ \frac{ft}{sec}$

FIGURE 6

1500Z 15 NOVEMBER 1955

$$\frac{\frac{Dp_a}{Dt}}{-p_a} \times 10^5 \text{ sec}^{-1}$$

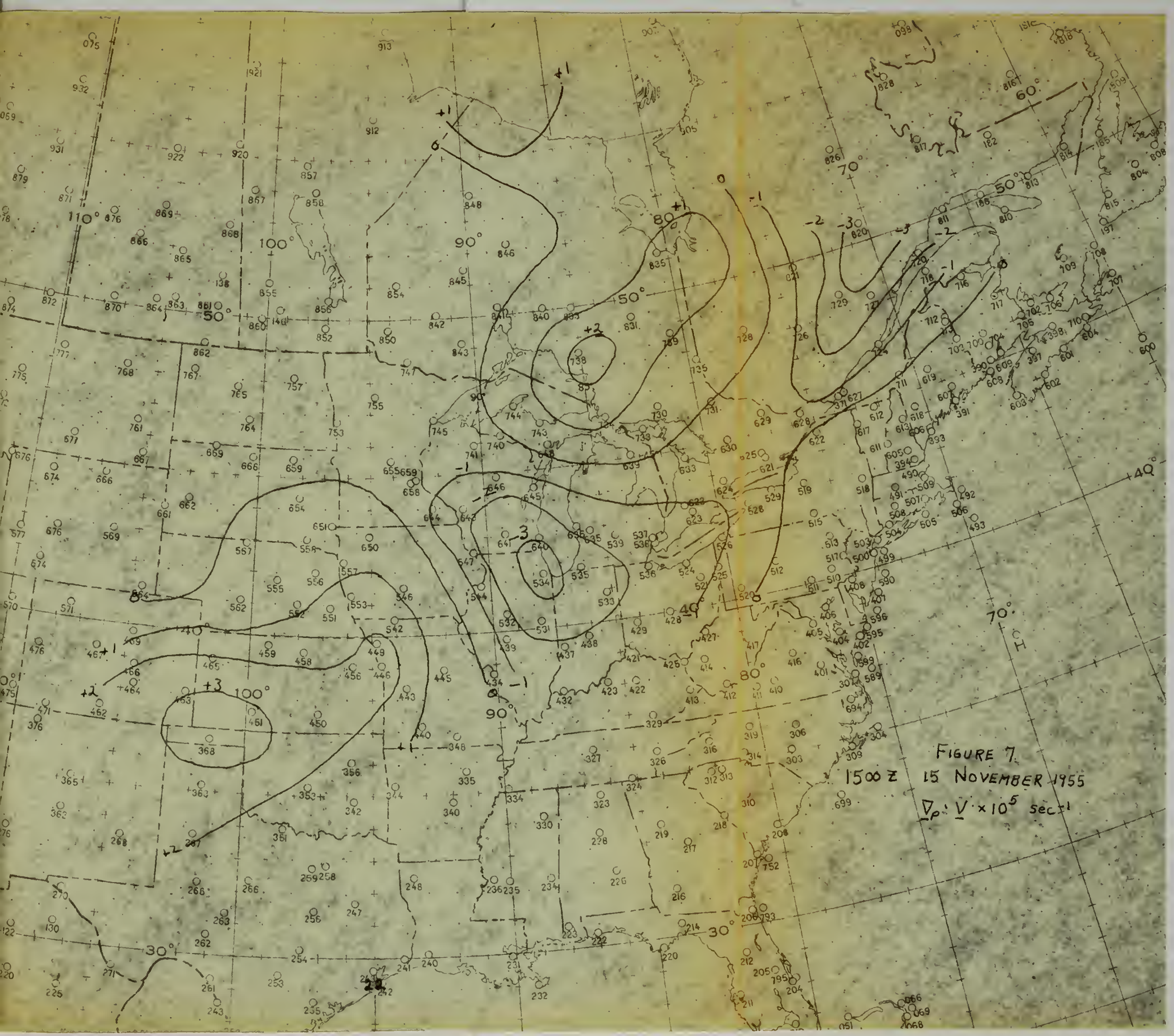

FIGURE 7.
1500 Z 15 NOVEMBER 1955
$\nabla_p \cdot \underline{V} \times 10^5$ sec^{-1}

SHORT-WAVE THROUGH AT 500 MB

FIGURE 8

0300Z 16 NOVEMBER 1955

$\frac{fd^2}{g} \frac{D\zeta_a}{Dt} \times 10^3 \frac{ft}{sec}$

SHORT-WAVE THROUGH AT 500 MB

FIGURE 9

0300Z 16 NOVEMBER 1955

$-\frac{fd}{dp}\int_a(\nabla_p \cdot \underline{V}) \times 10^3 \quad \frac{ft}{sec}$


SHORT-WAVE TROUGH
AT 500 MB
130°
120°
110°
100°
90°
80°
70°
60°
50°
40°
30°
25
FIGURE 10
0300 Z 16 NOVEMBER 1955
$\frac{Df}{Dt}$ x 10^5 sec^{-1}

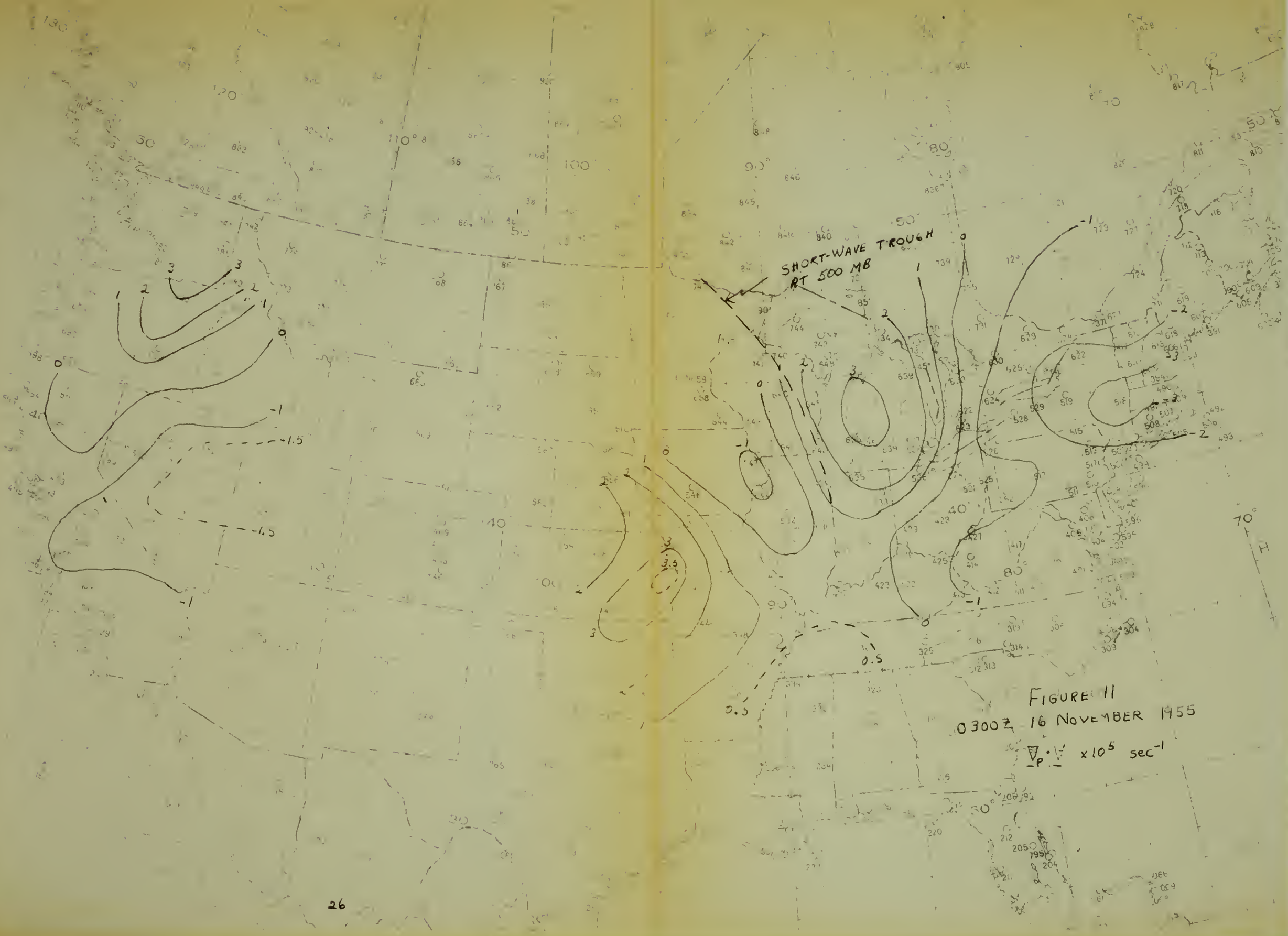

FIGURE 11
0300Z 16 NOVEMBER 1955
$\nabla_p \cdot \vec{V}$ x10^5 sec^{-1}

FIGURE 12
1500 Z 16 NOVEMBER 1955
$\frac{fd^2}{g}\frac{\partial g_a}{\partial t} \times 10^3$ $\frac{ft}{sec}$

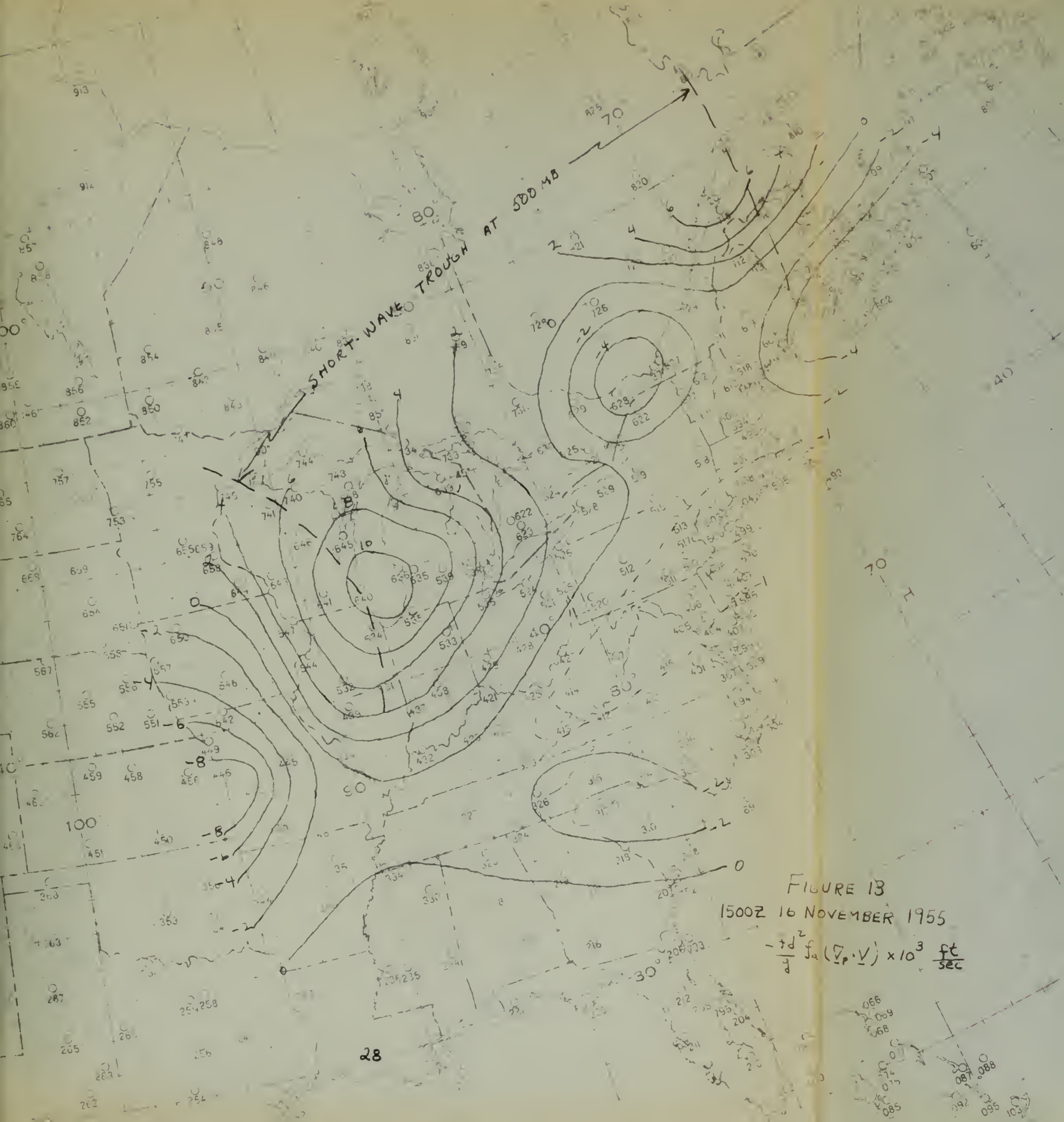

FIGURE 13
1500Z 16 NOVEMBER 1955
$-\frac{f^2}{g} f_a (\nabla_p \cdot \underline{V}) \times 10^3 \frac{ft}{sec}$

FIGURE 14
1500Z 16 NOVEMBER 1155

$$\frac{-\frac{\partial J_a}{\partial t}}{J_a} \times 10^5 \text{ sec}^{-1}$$

FIGURE 15
1500Z 16 NOVEMBER 1955
$\nabla_p \cdot \underline{V} \times 10^5$ sec^{-1}

Thesis
B32 Bechelmayr 35698
A study of divergence at
300 mbs.